Deep super-resolution imaging of thick tissue using structured illumination with adaptive optics

Jingyu Wang[1,2,*], Danail Stoychev[1,2,*], Mick Phillips[1], David Miguel Susano Pinto [1,2], Richard M. Parton[1], Nick Hall[1], Josh Titlow[1], Ana Rita Faria[1], Matthew Wincott[2], Dalia Gala[1], Andreas Gerondopoulos[1], Niloufer Irani[1], Ian Dobbie[1,3,#], Lothar Schermelleh[1,#], Martin Booth[2,#], Ilan Davis[1,#]

[1] Department of Biochemistry, the University of Oxford, Oxford OX1 3QU, UK.
[2] Department of Engineering, the University of Oxford, OX1 3PJ, UK.
[3] Current address: Department of Biology, Johns Hopkins University, Baltimore, MD-21218, USA
* Contributed equally to the work
[#] Authors for correspondence: ilan.davis@bioch.ox.ac.uk, martin.booth@eng.ox.ac.uk, ian.dobbie@jhu.edu, lothar.schermelleh@bioch.ox.ac.uk

Abstract

3D structured illumination microscopy (3D-SIM) doubles the resolution of fluorescence imaging and increases contrast in both fixed and live specimens. However, 3D-SIM has so far not been widely applied to imaging deep in thick tissues due to its sensitivity to specimen-induced aberrations, making the method difficult to apply beyond 10 µm in depth. Furthermore, 3D-SIM has not been available in an upright configuration, limiting its use for live imaging while manipulating the specimen, for example with electrophysiology. Here, we have overcome these barriers by developing a novel upright 3D-SIM system (termed DeepSIM) that incorporates adaptive optics (AO) for aberration correction and remote focusing, reducing artifacts, and removing the need to move the specimen or objective. Both these advantages are equally applicable to inverted 3D-SIM microscopes. We demonstrate high-quality 3D-SIM imaging up to 130 µm into complex tissue and live sample manipulation, including human cells and *Drosophila* larval brains and embryos.

Keywords

Super-resolution microscopy (SRM), 3D structured illumination microscopy (3D-SIM), aberration correction, deep imaging, adaptive optics (AO), deformable mirror (DM), remote focusing, spatial light modulator (SLM), neuroscience, nervous system, electrophysiology, *Drosophila*, live cell imaging

Introduction

Fluorescence microscopy has greatly advanced with the development of super-resolution microscopy (SRM) techniques that enable biological imaging with spatial resolutions well below the optical diffraction limit (Huang et al., 2009; Sahl et al., 2017; Schermelleh et al., 2019; Schermelleh et al., 2010). One of these approaches is 3D structured Illumination microscopy (3D-SIM) which features two-fold increased resolution in each spatial direction and enables fast optical sectioning with strongly enhanced imaging contrast. This approach recovers missing high spatial frequency information by illuminating the specimen with finely patterned illumination across the specimen (Gustafsson et al., 2008; Schermelleh et al., 2008). 3D-SIM has become increasingly popular amongst cell biologists, as it is compatible with standard fluorophores and labelling protocols commonly used in widefield or confocal microscopy.

Over the past decade, several off-the-shelf 3D-SIM instruments have become commercially available and have been successfully used for various biological applications. However, all share certain limitations that restrict their usage to thin specimens on inverted setups. Optical aberrations are a main contributor of common reconstruction artifacts in 3D-SIM imaging (Demmerle et al., 2017). These include (1) spherical aberration induced by refractive index (RI) mismatches between the immersion media, mounting media and sample, and (2) sample-induced aberrations caused by RI inhomogeneities within the specimen. As their deteriorating effects increase with imaging depth, it is currently difficult to obtain artifact-free 3D-SIM images at a depth greater than around 10 µm and over larger z-ranges in most specimens when using high numerical aperture (NA) oil-immersion objectives. Effective imaging depth may be extended to some extent using silicon-immersion objectives, which are designed for use with an immersion fluid with a refractive index closer to that of tissue, thus reducing spherical aberration. Currently, no upright, off-the-shelf SIM microscope systems exist that use water-dipping objectives, e.g. to carry out live neuroscience experiments with electrophysiology or other workflows involving imaging without a coverslip and providing access to the specimen and its manipulation while imaging. There are two reasons for this limitation. First, water-dipping objectives are more sensitive to aberrations than, for example, silicon immersion objectives due to refractive index mismatch and movement induced by living specimens. Second, the optical pathways of upright microscopes present technical challenges to the accommodation of 3D-SIM functionality together with the ergonomic constraints required to allow access to the specimen for

manipulation. Due to its rigid requirement of an optimal point spread function (PSF), 3D-SIM requires high mechanical stability, which potentially conflicts with the need for specimen manipulation for neuroscience experiments that require a large working distance and involve movement of the sample platform or instrument. Therefore, the benefits of 3D-SIM have not been utilized in large areas of biology, especially live cell imaging of nervous system preparations while manipulating the specimen.

An obvious solution to the above limitation is to incorporate adaptive optics (AO) using a deformable mirror (DM) in the optical path of a 3D-SIM microscope. AO would not only enable the correction of spherical and specimen-induced aberrations but also, allow remote focusing without the need to move the specimen or objective. These functionalities have been described as prototype methods for widefield (KAM et al., 2007), and 3D-SIM (Lin et al., 2021; Thomas et al., 2015; Turcotte et al., 2019; Žurauskas et al., 2019) as well as for remote focusing for multiphoton imaging (Žurauskas et al., 2017). However, none of the off-the-shelf 3D-SIM instruments are designed to allow the inclusion of AO. Moreover, AO hardware and software controls are currently not available as simple modules that can be added to the optical path of commercial systems. While some exciting bespoke-built AO-SIM systems have previously been described (Li et al., 2017; Lin et al., 2021; Thomas et al., 2015; Turcotte et al., 2019), these proof-of-principle prototypes use AO for aberration correction only and are not suitable for general biological applications and certainly not for applications requiring an upright optical configuration with multiple channels. To our knowledge, DM-driven remote focusing although well studied in both simulation (Kner et al., 2011) and experiments for example, confocal (Poland et al., 2008) and multiphoton imaging, has not be implemented on any 3D-SIM systems.

Here, we describe our bespoke upright 3D-SIM prototype microscope system with integrated AO, enabling deep imaging in live wholemount biological specimens, while manipulating the specimen (Fig. 1). The system is based around a 60x/1.1 NA water-dipping objective for which we demonstrate high-quality 3D-SIM with nearly two-fold spatial resolution extension in three dimensions at depths from a few µm up to 130 µm deep. We use AO not only for sample-induced aberration correction for deep tissue imaging, but also for remote focusing, which enables fast transitions of the imaging plane and prevents pressure waves caused by the motion along the optical axis of the specimen or the objective lens. Our novel approach and instrument design enables simultaneous multichannel imaging in conventional and super-resolution modes, with acquisitions of fast Z-stacks and timelapse, deep in live specimens while keeping them accessible to experimental manipulation. The modular design and user-friendly open-source Python software of DeepSIM (see Material and Methods for

further details) allow for convenient sample navigation and a simple workflow for routine biological experiments. We first verify the system performance using beads and cells in culture. We then apply the full range of novel imaging modalities available on DeepSIM to a wide range of specimen types, from mammalian tissue culture cells to *Drosophila* larval brains and embryos. Finally, although our use of AO for aberration correction and remote focusing is demonstrated on an upright microscope with water dipping objectives, the principles we have established could be applied equally to an inverted 3D-SIM system to extend the depth of imaging considerably and allow more rapid acquisition of 3D stacks without the need to move the specimen or objective.

Results

To initially assess the baseline performance of DeepSIM in applications where there are minimal aberrations, we imaged 100nm diameter green-fluorescent beads. We used 3D images of beads to estimate the PSF in all imaging modalities (Fig. 2 A and B). We first compared the performance in widefield in two configurations. First, standard Microscope optics without AO correction by using a DM-bypass (BP) optical path (shown as BP WF; see Methods) and second, with AO correction for system aberrations (shown as AO WF; see Methods). We expected minimal aberrations to affect images of beads mounted under a coverslip following careful adjustment of the collar of the objective designed for correcting spherical aberration. Correspondingly, we found that in the wide-field (WF) mode, using AO to correct system aberrations led to a small improvement in the overall shape of the PSF compared with the standard WF using BP. This improvement was evident when measuring the FWHM of the PSF in the X and Z direction, which changed from 286 nm and 970 nm, respectively, in BP WF to 281 nm and 901 nm in AO WF (Fig. 2 A and B). Next, we acquired equivalent results using the DM to change the microscope's plane of focus, which we called remote focusing (RF) (Materials and Methods) and compared these measurements to those from conventional acquisition of a z-stack with a piezo Z stage. Widefield RF imaging results in PSFs with a FWHM resolution that is very close to that using AO system correction or DM-bypass, namely 282 nm and 848 nm respectively (Fig. 2 A and Fig. 2 B as RF WF). However, when we acquired images of the same specimens using 3D-SIM, we obtained the smallest PSFs amongst the four experiments, with a FWHM of 176nm in XY and 566nm in Z. This resolution enhancement is approaching the expected limit of half of the calculated widefield diffraction limits of 281 nm (in XY) and 851 nm (in Z) for an NA of 1.1, of the water dipping objective used. These FWHM values are higher than the optimum expected for SIM, as we chose the linewidth of the structured illumination pattern, conservatively, to be 310 nm

larger than theoretical optimal value 285 nm to avoid accidental clipping on the DM (see materials and methods for details).

3D-SIM, like other super-resolution methods, is sensitive to low levels of system and specimen-induced aberrations, even at a depth typical of single cells in culture. Such minor aberrations tend to be insignificant in conventional microscopy modalities such as widefield and confocal (Wang and Zhang, 2021). Therefore, we first verified the degree of resolution enhancement by 3D-SIM in mammalian tissue culture COS-7 cells (Fig. 2, C left, shown in blue) with microtubules labelled with AlexaFluor 488 and in another example, endoplasmic reticulum Rtn4 labelled by AlexaFluor 555 (Fig. 2, C right, shown in amber). Comparing to the wide-field and 3D-SIM images shown side-by-side, the optical sectioning capability of 3D-SIM is easily noticeable at the large difference in out-of-focus signal in Fig. 2 C, especially in the XZ cross-section view displayed below the XY views. The resolution enhancement can also be confirmed in the Fourier space as shown in Fig. 2D, where the wide-field power spectrum's energy is mostly concentrated in the central area, the SIM data presents a much more even distribution across the frequency space, extended to the high frequency region beyond 200 nm. Because of the high spatial information carried by the microtubule structures, a radial integration of the 2D power spectrum provides a close estimation of the system OTF where lateral resolution can be measured; they were measured to be 330 nm and 187 nm, respectively for wide-field and SIM modes, close to the FWHM values measured from beads data shown in Fig. 2, A. We also imaged mammalian tissue culture COS-7 cells in the red channel with endoplasmic reticulum Rtn4 labelled by AlexaFluor 555 (Fig. 2, C right, shown in amber). The performance of the system is similar in the green channel, except the absolute spatial resolution is lower due to the longer wavelength. The resolutions measured from the Fourier power plots in wide-field mode and 3D-SIM mode are 403 nm and 208 nm, respectively.

A significant benefit and uniqueness of the DeepSIM design is its upright configuration, whereas commercial SIM systems are built around inverted microscopes. The DeepSIM system is therefore applicable to tissue-based imaging and live experiments such as electrophysiology, whereas many other SIM instruments are restricted to imaging thin samples, such as cultured cells. We evaluated the applicability of these unique capabilities of the DeepSIM microscope to thick biological specimens that have a substantial degree of refractive index inhomogeneity, leading to optical aberrations. We used AO in conjunction with 3D-SIM to image thick and complex tissues of the fixed *Drosophila* larval neuromuscular junction (NMJ) preparation. We imaged larvae from a transgenic line expressing a bright GFP protein trap of the cell-cell "septate" junction protein Neurexin IV (Nrx-IV), at a depth of

5-15 µm (Fig. 3) (see details in Methods, fly lines). The AO-corrected volume images showed significant improvements in both intensity and contrast after reconstruction, compared with uncorrected images (Fig. 3). The improvement was especially noticeable between the XZ views in Fig. 3 A and B, as the major effect of aberrations is to distort the PSF along the optical axis. This is particularly the case for the dominant spherical aberration, which elongates the focus along the axis, but is also an effect of other aberration modes, such as coma, which typically lead to a bending of the PSF in cross-section view (see details in Supplementary section 3).

To further test the microscope's performance at greater depth, we imaged dissected and formaldehyde fixed *Drosophila* larval brains, which are up to 130 µm thick. We imaged both the top and bottom layers of the thickest part of the brain lobe of brains mounted between a standard microscope coverslip (#1.5) and a slide. To help visualize the effects of aberrations and evaluate the ability of AO to correct them at depth, we placed 100 nm diameter red fluorescent beads (580/605 nm) both on the coverslip and on the glass slide underneath the tissue. We imaged the beads 3 µm below the cover slip as well as at a depth of 133 µm, which required focusing through the entire volume of the mounted brain (Fig. 4). We found that AO aberration correction was essential for obtaining interpretable images of the beads and cells through the brain to the other side (Fig. 4 A and B). Control deep images where the AO is bypassed suffered from severe aberrations, where the cell membranes could not be observed as continuous structures (Fig. 4, C) and large artefacts are present in the reconstructed images. In contrast, imaging at the same depth using AO correction of 24 aberration modes (Zernike aberration modes Z4-Z28; see details in Supplementary AO methods section) enabled 3D-SIM reconstructions to produce clearer 3D images with reduced artefacts and enhanced contrast. Large areas of the cell membranes could be visualized showing the expected overall structure. The effect of aberrations and their correction can be confirmed and visualized particularly clearly in the red channel where individual bead images closely mimic the shape of the local PSF while the equivalent image without AO present large unrecognizable structures. The aberration correction method employed here effectively estimated a correction averaged across the entire FOV of 68 x 68 µm at 130 µm depth. It is often the case deep in tissue that the aberrations vary across the field, so that an average correction results in residual aberrations in some regions. Consequently, some variation can be observed within the bead images in Fig. 4, D. However, the overall PSF shapes as shown in Fig. 4 D were dramatically improved by the AO compared to the equivalent without AO in Fig. 4 C. The peak intensity and SNR with AO are significantly higher than the results without AO, as plotted in Fig. 4 E.

Biological samples, even flat cells in culture, are usually thick enough to induce substantial aberrations which vary considerably throughout the volume of a specimen. Therefore, effective correction needs to be modified with depth, while acquiring volumetric images. As the DeepSIM system is capable of rapidly changing the focal position through remote focusing, we demonstrated combining remote focusing with AO aberration correction on cells in culture (Fig. 5). In principle, it would be possible to perform aberration measurements at every imaging plane within the volume. However, such an approach requires a long measurement time before each acquisition, which might lead to unnecessary photobleaching. As we found that the aberrations change approximately linearly in depth, we could measure the aberration in two planes and calculate the corrections in intermediate planes by interpolation, an approach which we named, “Multi-position AO”. To test multi-position AO, we imaged fixed COS7 cells in culture stained for microtubules, to visualize the spindles during mitosis. We measured the aberrations at the top and the bottom of the cells and then applied an interpolated correction at different Z positions in between the two measured planes. Our results show conclusively that remote focusing with aberration correction produced images with improved contrast and resolution compared to remote focusing without aberration correction. The improvements provided by interpolated aberration corrections were particularly noticeable in point-like structures in the specimens (Fig. 5, D). In contrast, such points result in elongated structures when imaged without aberration correction (Fig. 5, C). Fig. 5, E displays the image intensity of two line profiles in X and Z directions without and with multi-plane AO for comparison, demonstrating increase of the signal intensity with AO correction in addition to the resolution improvement. In the case of the X plot, shown in Fig. 5, E, although two peaks can be separated without AO, indicated by the red arrows, the distance is enlarged compared to that in the image with AO. This is because the aberration distorts the sample spatial structure, which can be observed in in the 3× zoomed inset in Fig. 5, C; while the same structure is correctly revealed in the AO corrected results, shown in Fig.5, D, zoomed inset.

One of the challenges of 3D-SIM has been its limited ability to carry out live cell imaging rapidly and in thick specimens (Gao et al., 2012). Living specimens are particularly challenging for two reasons. First, the structures can change within the time it takes to acquire 3D volume. And second, imaging through living material causes more pronounced aberrations compared with fixed material, in which the refractive index is made more homogenous and higher by introducing a high refractive index mounting medium, such as Glycerol. The DeepSIM approach has the potential to resolve both these difficulties. First aberration correction can, in principle, be used to correct more severe aberrations. And second, using our interpolation approach to calculating the shape of the mirror required to

correct aberrations rather than measuring the shape, is much faster, enabling faster SIM to match dynamic biology.

To test the feasibility of 3D-SIM for dynamic live biological imaging, we imaged *Drosophila* embryos undergoing rapid mitosis (Fig. 6). We collected eggs from transgenic animals expressing the microtubule binding protein Jupiter fused to GFP and histoneH2A tagged with RFP. The histone H2A::RFP; Jupiter::GFP eggs we dechorionated and mounted in aqueous solution in order to image chromosomes and microtubules simultaneously, during mitotic division in the syncytial blastoderm stages of early *Drosophila* embryos. We used remote focusing to repeatedly acquire two-color image volumes at a depth of 5 µm under the surface at a rate of 20 fps, equivalent of 10 seconds per 3D volume (two-color) at room temperature for 6.5 minutes. Each volume of 26.4 x 21. 12 x 0.875 µm requires 210 raw images for 3D-SIM reconstruction. Using AO based aberration correction with interpolation combined with remote focusing we were able to obtain an effective time sequence of 3D-SIM stacks with reduced residual aberrations. Wide field and Z-projections of three volumes were hand-picked to show the moments before, during and after cell divisions at 0, 55 and 102 seconds in the sequence (Fig. 6 A, B, C and D, E, F respectively). Seven different Z positions from the first volume are displayed in Fig.6 G-M. The results demonstrate that the remote focusing function of the system can be used for live 3D-SIM experiments, allowing four-dimensional acquisition while keeping the specimen stationary and thus avoid the usual agitation and perturbations associated with mechanical translation.

Discussion

We have shown how the design of DeepSIM, as a prototype upright super-resolution microscope with integrated AO, allows effective 3D super-resolution imaging to a depth of at least 130 µm in thick complex tissues. Its modular design and open-source Python software, for both system control and GUI (see details in Material and Methods/ Software), make it user-friendly and versatile. These design concepts allow the adaptation of the instrument to suit specific research applications and enable protocols for experiments at scale. The upright optical design, combined with aberration correction and remote focusing, means that the instrument is particularly suited for applications that require super-resolution live imaging of thick tissue, organs or whole organisms. Importantly, the design is compatible with specimen manipulation, such as microinjection, carrying out electrophysiology measurements, or adding reagents to specimens during imaging experiments. In this study we have established a new paradigm for 3D-SIM to be applied at depth while acquiring volumes without moving the specimen or the objective, while varying the aberration corrections

across the acquired volume and in a depth-specific manner. This general principle can now be applied to any SIM configuring, including an inverted pathway, which can make use of the highest possible NA objectives, obtaining a 3D volume at depth with the maximally possible resolution of SIM after reconstruction.

Current commercially available 3D-SIM instruments are mostly based around inverted microscopes and high NA oil immersion objectives that are susceptible to aberrations when focusing into any specimens with RI mismatch, so frequently only produce good images up to depths of a few µm. When such instruments are used with silicon immersion objectives, with slightly reduced NA, high-quality SIM can be extended to a depth of around 20 µm (Ogushi et al., 2021; Richter et al., 2019). In all cases objective correction collars can only effectively minimize spherical aberrations for SIM imaging in a single channel. For multi-color imaging, not only the mounting media needs to be selected for minimal RI mismatch for average wavelength of all imaging channels, wavelength specific fine-tuning of the mounting medium RI is also required (Demmerle et al., 2017; Wang et al., 2018). Therefore, for most practical purposes, these microscopes can only effectively be applied to thin single layers of tissue culture cells on microscope slides or only to the superficial surface of complex tissues that are relatively optically transparent. Furthermore, they are not readily adapted to imaging regimes requiring the specimen and objective to remain motionless while imaging. Hence, DeepSIM fills an important application gap for deep imaging in live multi-cellular tissue. The method opens up new possibilities for future biological investigations, such as super-resolution imaging in live specimens or whole animals, imaging fast live 3D time-lapse movies while carrying out specimen manipulations, for example, micro-injection into *Drosophila* embryos, or carrying out electrophysiology measurements on living mouse brain sections or *Drosophila* NMJ preparations while imaging.

The range of remote focusing shown in this work was limited to ±5 µm, which is smaller than some previous demonstrations. There were two reasons for the choice of this range. First, the deformable mirror can only reliably produce PSF with minimal aberration repeatedly in this range (see supplementary, Deformable Mirror section). Second, for 3D-SIM acquisition, 10 µm is a commonly used Z range. Especially in multi-color imaging, a rather large number of images, about 1200 frames per channel, would be required. While larger volume acquisition is possible, it would lead to considerable photo-bleaching, and longer acquisition and reconstruction time. Moreover, there is a trade-off between the number of volumes that can be acquired (number of time points) and the number of Z-sections within the volume.

The resolution achieved with DeepSIM was 176 nm (full width at half maximum, FWHM) at 488 nm using a water dipping objective with an NA of 1.1. In comparison, inverted commercial 3D-SIM instruments routinely achieve 100-120 nm resolution at 488 nm using a high-NA oil immersion objective. While the DeepSIM resolution is therefore lower in absolute terms, this was a design trade-off chosen to make the microscope compatible with live imaging in an upright configuration and with a large working distance. Hence, it is more pertinent to compare the resolution of DeepSIM to that achievable for live cell imaging in widefield microscopy, using the same NA water dipping objective, which is 286 nm in the green channel and 336 nm in the red channel. However, the fundamental design of the DeepSIM microscope could be readily adapted, if necessary, to work in upright or inverted mode with other objective lenses, including oil or silicone immersion objectives to achieve higher spatial resolution, while still benefitting from the use of AO for motionless deep imaging. In these cases, the working distance would be compromised, making it much more difficult to manipulate the sample, for example by microinjection or with electrophysiology needles. Nevertheless, the implementation of AO hardware and software described in this report, is suitable for most widefield-based instruments, including SIM that would benefit from the incorporation of a DM, but only when a DM can easily be added to the optical path. Although DeepSIM's design was mostly optimized for upright microscopy and tissue specimens, it can also benefit other similar microscopes. Notably, CryoSIM (Kounatidis et al., 2020), would hugely benefit from inclusion of AO to correct aberrations induced by inhomogeneous refractive index of air at cryogenic temperatures.

There are various routes through which the system performance could be enhanced in future versions of DeepSIM. First, the speed of acquisition in the reported demonstration was limited by a few key system components, which could be improved in future developments. A key limiting factor in widefield mode was the EM-CCD camera. The best overall performance in terms of structured illumination modulation was achieved when using conventional CCD modes. However, due to the data transfer time (3 MHz pixel readout rate), the frame rate was limited to about 100 fps for a reasonable size field of view. This acquisition speed could be increased by using newer sCMOS cameras. Second, for SIM acquisition, imaging speed was also limited by the SLM update rate, determined by the settling time of the nematic liquid crystal technology (around 20-40 ms), giving a maximum frame rate of 50 fps raw data. Fast SLMs using ferroelectric liquid crystal materials have been demonstrated in SIM for high-speed SIM imaging (Lin et al., 2021), though it is more challenging to use such SLMs for multi-color imaging, as the phase modulation is binary and hence optimized for a single wavelength. Third, future improvements could also include the incorporation of denoising algorithms into the reconstruction process to allow lower light

dosage, which would enable faster imaging, lower bleaching, and reduced specimen photodamage. Combinations of such hardware and software improvements would enhance acquisition speed for realistic experimental situations imaging live biological processes in super-resolution at high volumetric rates. Finally, in the future the optical path of DeepSIM could be simplified and reduced in size, thus making it easier to adopt or commercialize, as well as building specific DeepSIM systems designed for bespoke applications.

Material and Methods

Microscope platform

We based the DeepSIM system on our previous bespoke Cryo-SIM (Phillips et al., 2020). The microscope body is built in an upright configuration, as illustrated in Fig.1, and it is designed around a water-dipping objective lens (Olympus LUMFLN60XW), which was selected for imaging of tissues, particularly for *Drosophila* brain, NMJ, and electrophysiological experiments. With the goal of flexibility and ease of use, especially to assist fast and accurate sample navigation, we also included a low magnification dry lens (Olympus LMPLFLN10X). The objective lenses were mounted at fixed positions and the sample was translated in 3D by a set of X, Y, and Z stages. Images from the two objective lenses were mapped in 3D so that the same sites could be revisited with minimal error by both objective lenses. The XY translation was handled by a large opening motorized stage (PI M-687.UN) and the Z translation was handled by a combination of a heavy-duty linear stage (Aerotech PRO115) and piezo stage (PI P-736.ZCN) for accurate and fast motion during experiments. The microscope body was connected optically to the rest of the system with a periscope (see details in Supplementary Fig. S1 and Fig. S3).

Structured illumination

To implement 3D SIM, we adopted mid-speed analogue SLM (Boulder Nonlinear Systems, HSP512-488-800) to produce structured illumination. The SLM was positioned in sample-conjugated plane and linear sinusoidal patterns were generated for three orientation angles. The $\pm 1^{st}$ order and zero order beams were used to interfere at the sample plane to generate the 3D structured illumination. To achieve optimal interference contrast, the linear polarisation of excitation beam from the SLM was rotated using a liquid crystal device (Meadowlarks Optics, LPR-100-λ) to maintain S polarisation at the incident plane at the back pupil of the objective lens at each SI orientation. For widefield acquisitions, the SLM was switched off and used as a single reflector so that only zero order beam provides epi-illumination; while for SIM acquisition, the SLM was switched on and it was preloaded with

the SI patterns that are generated according to the user specified wavelength and line width in the software before acquisition. During data acquisition, the SI phase and angle were rotated in a fixed sequence, synchronised with the polarisation rotators, the light sources, and the cameras.

Deformable mirror

Sensorless AO was chosen for the correction of aberration, as it is simple and effective to implement (Žurauskas et al., 2019). A deformable mirror (Alpao DM69-15) was positioned at the back-pupil conjugated plane, between the main dichroic filter and the microscope body, so that the DM was used for correcting both the excitation and emission paths. The DM aperture was matched to cover the back-pupil of the objective lens by relay optics (L1-L4 in Suppl. Fig1). An integrated interferometer was used to calibrate the DM for both aberration correction and remote focusing (optical path illustrated in yellow dotted line in Fig. S1). A pair of flip mirrors were included to create an optical path that bypassed the DM (referred to as the “DM-bypass” path), to permit easy comparison between conventional imaging and that with AO aberration correction.

Software

System control software package was composed of three parts, as illustrated in Fig.1 b,: *python-microscope* for low level hardware driving for the whole optomechanical system (Susano Pinto et al., 2021), *microscope-cockpit* for a user interface and experiments (Phillips et al., 2022), and *microscope-aotools* for performing DM calibration and AO correction (Hall et al., 2020). All three were further developed and improved, find links to the latest repositories in the supplementary software section for details. For SIM data reconstruction, we used a commercial package softWoRx (GE Healthcare). OTF required for reconstruction for each imaging channel were generated from experimental data acquired from a single fluorescent bead. Multi-color image alignments were performed in open-source software Chromagnon (Matsuda et al., 2020). SIM characterization was done with SIMcheck (Ball et al., 2015). General image processing was done in Fiji (Schindelin et al., 2012).

Sensorless AO

Model-based approaches for adaptive optics were used for wavefront control. The DM was calibrated to generate control metrics that delivered accurate wavefronts in Zernike modes (Antonello et al., 2020). An integrated interferometer was built into the optical path that could be folded into the microscope when required. A Zernike modes quality check was implemented in *microscope-aotools* and regularly used to verify the accuracy of the DM. A

Fourier domain image metric was used for optimizing each Zernike mode, for specimens with structures of sufficiently high spatial frequency (Hall, 2020) . When the spatial frequencies were not high enough, ISOsense (Žurauskas et al., 2019) was adopted to achieve a more robust AO correction.

Multi-plane aberration correction

We used multi-plane aberration correction to compensate for the optical distortions in thick volumes. We applied our standard sensorless AO routine at fixed positions, e.g. at the top and the bottom of the volume, and then we fitted the resulting correction Zernike coefficients to a linear fitting, assuming the refractive index changed in a linear manner with Z within the range. This simple presumption allowed us to calculate in advance the corrections required at every section of the volume. All patterns necessary for an experiment were registered to Z location and queued on the DM device and then TTL triggers were used in real-time to cycle through the patterns while updating imaging position either with piezo Z-stage or DM driven remote focusing.

Remote focusing

Remote focusing is highly desired in neuronal imaging and other experiments, such as electrophysiology, where it is required that the sample remains stationary during acquisitions. AO can be used to replace piezo Z stage (Žurauskas et al., 2017). We added defocus to the aberration correction pattern and the two worked completely independently. To calculate the required remote focusing patterns we first performed a calibration experiment where we used a sample with a single layer of fluorescent beads. The sample was displaced by the piezo Z stage first in one direction and then by the same amount in the opposite direction. Sensorless AO correction was used at both positions to correct for Zernike modes #4 (defocus) to #22 (secondary spherical). We then performed a linear fit to the correction coefficients and used this model as a look-up table to calculate the remote focusing pattern for all Z positions. This approach achieved a linear response with high precision on the Alpao DM69-15 within a range of 10 µm however the scaling accuracy was found not perfect. This is not surprising to us as this DM is known to have a creep effect (Bitenc et al., 2014). The dynamic characteristics of the device are discussed in more detail in the Supplementary Material. We found that in practice the response can vary by a scale factor related to the speed with which the DM shape was varied. To determine this scaling factor, we established a second calibration step where the piezo Z stage was used as a

reference to displace the sample of beads in Z and provide ground-truth values. While performing the scale calibration, we matched the displacements with the remote focusing that is interpolated from the linear fitting and the displacement by Z-stage. Taking measurement of a number of points in the remote focusing Z range. We then fitted a linear relationship between remote focusing Z and piezo stage Z is established and its slope was used as the scaling factor that is multiplied with Z value using the first step to achieve accurate remote focusing. Similar to multiple point AO correction, before imaging experiments, all remote focusing patterns were computed in advance, added to the aberration correction patterns if required, and queued on the DM driver. TTL triggers were then used to cycle through all queued patterns and to synchronize with the rest of the hardware.

Cell culture

COS-7 (ATTC) cells were grown on no. 1.5 glass coverslips in DMEM containing 10% fetal bovine serum (Sigma-Alrich), washed twice with 2 ml of 100 mM sodium phosphate, and fixed for 2 h in 2 ml PLP (2% [wt/vol] paraformaldehyde in 87.5 mM lysine, 87.5 mM sodium phosphate pH 7.4, and 10 mM sodium periodate). Coverslips were washed three times in 2 ml (100 mM) sodium phosphate, pH 7.4, before permeabilization in 1 mg/ml BSA, 0.05% saponin, and 100 mM sodium phosphate, pH 7.4, for 30 min. In all cases, primary antibody (a-TOMM20 (mouse 612278, BD) AF488 and Rtn4 (rabbit; AbD Serotec) AF555) staining was performed in 1 mg/ml BSA, 0.05% saponin, and 100 mM sodium phosphate, pH 7.4 for 60 min at room temperature. Affinity-purified antibodies were used at 1 µg/ml; commercial antibodies were used as directed by the manufacturers. DAPI was added to the secondary antibody staining solution at 0.3 µg/ml. Coverslips were mounted in Mowiol 4-88 mounting medium (EMD Millipore).

Fly strains

The following fly lines were used in this study. Nrx-IV::GFP (CA06597, kindly gifted by the Rita Teodoro lab) for the NMJ samples, cno::YFP (CPTI000590, DGRC 115111) for the brain samples, Jupiter::GFP, histone::RFP (Hailstone et al., 2020) for embryos. All stocks were raised on standard cornmeal-based medium at 25C.

Fixed Drosophila larval fillet for imaging of neuromuscular junctions

The NMJ samples were prepared by following the protocol in (Brent et al., 2009), apart from the fixation, which was done in 4% paraformaldehyde (PFA) in PBSTX (phosphate-buffered saline with 0.1% Triton X-100) for 30 minutes and then followed by two washes for 20

minutes each in PBSTX. The samples were then incubated with Cy3-conjugated α-HRP antibody (1:500, Jackson ImmunoResearch 123-165-021) for 1 hour. Finally, the samples were washed in PBSTX for 45 minutes and then mounted in Vectashield. All steps were done at room temperature.

Fixed whole *Drosophila* brains

Third instar *Drosophila* larvae were dissected in PBS. Brains were removed and fixed in 4% PFA in PBSTX (0.3% Triton X-100) for 25 minutes. Afterwards, they were rinsed three times in PBSTX, further permeabilized with two 20-minute washes, and then mounted in PBS.

Drosophila embryos for live imaging

The live embryo samples were prepared as described in (Parton et al., 2010), except that they were mounted in PBS.

Acknowledgements

John Sedat for the original optical design, similar design is described in (Phillips et al., 2020); Antonia Göhler and Mantas Žurauskas for the initial optical characterization, work which was published previously; Martin Hailstone, Francesca Robertson, and Jeff Lee for preparing specimens during various phases of using the DeepSIM instruments with biology, imaging that was not shown in the manuscript. JW thanks Jacopo Antonello, Chao He and Jiahe Cui for insightful discussions and advice for AO devices. We are grateful to Micron Oxford and its numerous partners and staff for discussions and providing the environment required for the success of this complex interdisciplinary technology development project.

Funding

DSP, IMD, ID, MP, NH, and RMP were funded by Wellcome Trust (091911/Z/11/Z, 096144/Z/11/Z, 105605/Z/14/Z, 107457/Z/15/Z, 203141/Z/16/Z, 209412/Z/ 17/Z). JW, MW, and MB were funded by European Research Council (AdOMiS, No. 695140). DS was funded by a BBSRC iCASE studentship to ID and MB sponsored by Aurox. The research was also supported by Medical Research Council grant [MR/K01577X/1] to ID.

Author Contributions

AG – Andreas Gerondopoulos
DG – Dalia Gala
DS – Danail Stoychev
DSP – David Susano-Pinto
IMD – Ian Dobbie
ID – Ilan Davis
JT – Josh Titlow
JW – Jingyu Wang
LS – Lothar Schermelleh
MB – Martin Booth
MP – Mick Phillips
MW – Matthew Wincott
NH – Nicholas Hall
NI – Niloufer Irani
RF – Rita Faria
RMP – Richard Parton

Original vision and concept development: ID, IMD, RMP.
Designed the microscope optics: ID, IMD, MP.
Designed and implemented the optomechanics: MP.
Implemented electronics: DS, MP, IMD.
Implemented initial optical system: IMD, NH, MP.
Development of control software: DS, MP, IMD, DSP, NH, MW, JW.
Developed adaptive optics methods, algorithms and calibration: NH, JW, DS, MB.
Implemented remote focusing method: JW, DS.
Acquisition of initial data: IMD, NH, JT, RMP.
Refined and reimplemented optical system and adaptive optics control: JW, DS.
Refined experimental processes: JW, DS, LS, RF, RMP.
Experimental strategy and preparation of specimens: JW, DS, LS, RP, RF, AG, NI, DG, RMP.
Imaging experiments, calibration, and data processing: JW, DS, LS.
Article conceptualisation: ID, LS, JW, DS, MB, RMP.
Initial draft of article and figure preparation: ID, DS, JW.
Revision of article: ID, LS, JW, DS, MB, IMD.
Obtaining funding: ID, MB, LS.
Supervision: IMD, ID, MB, LS.

Figures

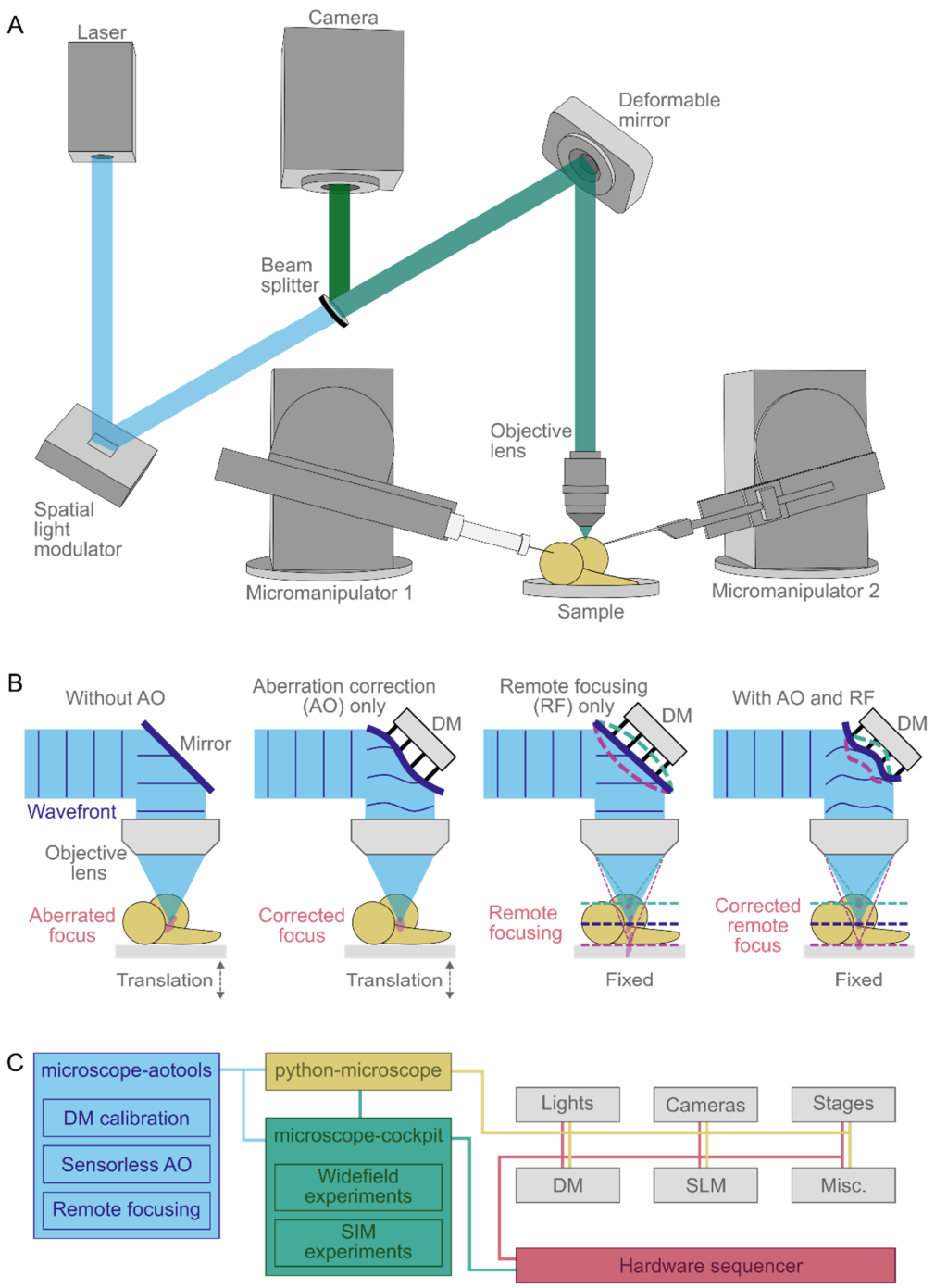

Figure 1. Simplified overview of the DeepSIM setup. (**A**) The optical arrangement showing DeepSIM's configuration as an upright microscope, which allows the use of micromanipulators for applications such as microinjection and electrophysiology. The illumination is incident on a spatial light modulator (SLM), which is conjugate to the object/image plan, then reflected off a deformable mirror (DM) before being passed through

to the sample via an objective lens. In the imaging path, the reflected fluorescence is coupled off via a dichroic beam splitter (BS) and then collected by separate cameras for each channel. (**B**) Different imaging modes are enabled in parallel on DeepSIM. Deep imaging without AO usually leads to an aberrated PSF due to RI mismatch and sample inhomogeneity. Sensorless AO correction compensates for sample-induced aberrations. Remote focusing (RF) enables fast focusing at varying depths without moving the specimen/objective. Coupling AO and RF produce aberration-corrected imaging at different depths, without mechanical movement. (**C**) DeepSIM is controlled by Cockpit, which consists of 3 packages: python-microscope is responsible for the control of all hardware devices; microscope-cockpit provides a user-friendly GUI; Microscope-AOTools provide adaptive optics control to both aforementioned packages. The system uses a hardware sequencer, Red Pitaya 125-14, to coordinate different instruments for image acquisition with structured or wide-field illumination.

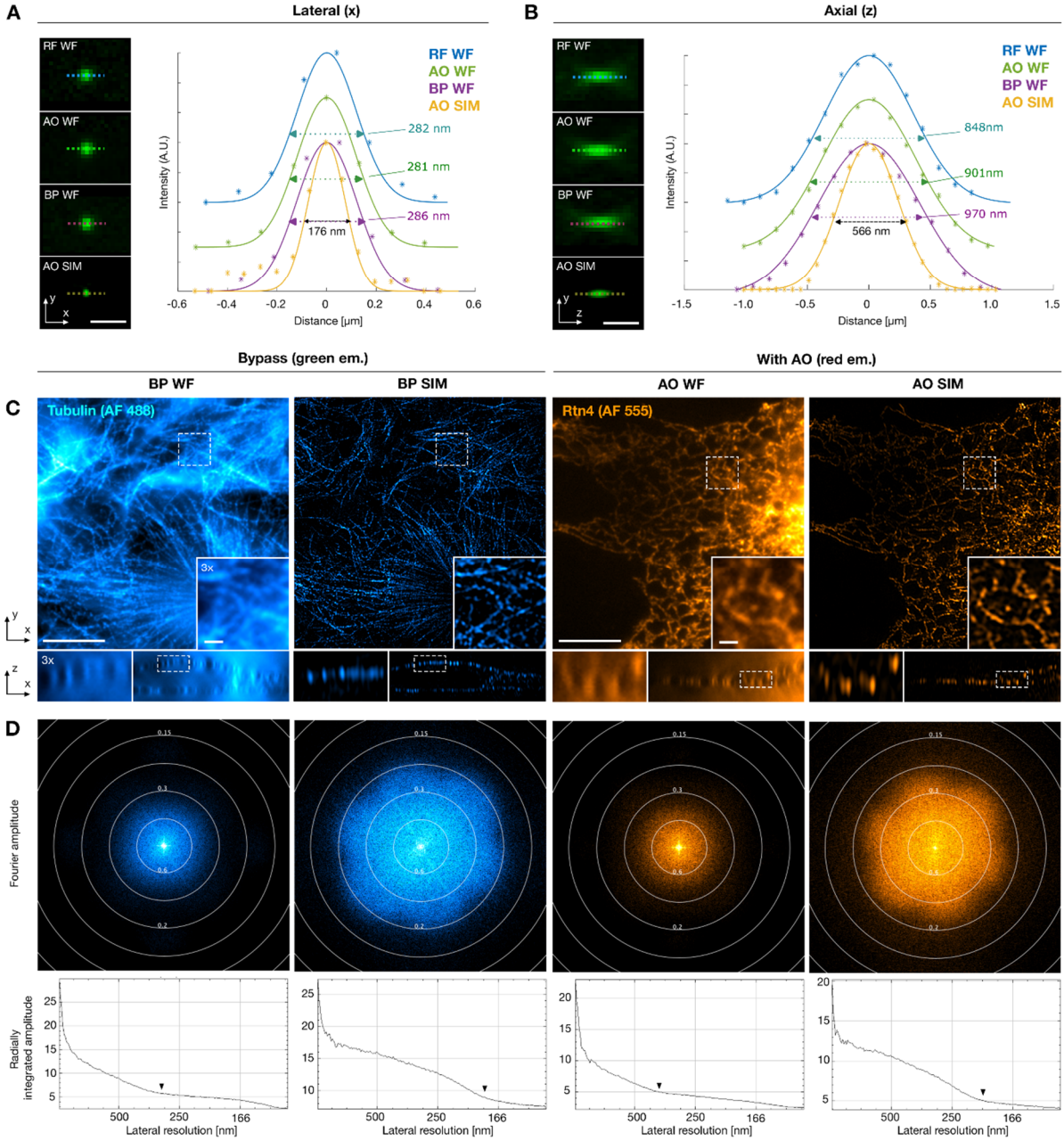

Figure 2. Characterization of the DeepSIM system. Lateral (**A**) and axial (**B**) point spread functions (PSF) for the different modalities of the instrument measured from 100 nm green-fluorescent beads. Widefield DM-bypass (BP WF), widefield with AO (AO WF), widefield with aberration correction and remote focusing (RF WF), and 3D-SIM with AO (AO SIM). The images in XY plane and the XZ plane with a plot of the PSF at the peak in X and Z direction are displayed from left to right. Scale bar: 500 nm. (**C**) Wide-field (WF) and 3D-SIM images acquired from COS-7 cells in XY and XZ view, which show structures of microtubules in the green channel (shown in blue) and endoplasmic reticulum in the red channel (shown in amber); the dotted boxed areas in all images are shown in 3x zoom in subsets. (**D**) Fourier amplitude in XY spatial frequency space, where spatial information enhancement due to SIM

can be observed from the wide-field data (left) to the SIM data (right) in green and red channels. Radially integrated amplitude of XY Fourier projection of wide-field and SIM (right) are displayed underneath, where highest achieved resolution is measured and indicated by black arrows. Total volume: 31.68 x 31.68 μm^2. Scale bar: 100 µm.

620

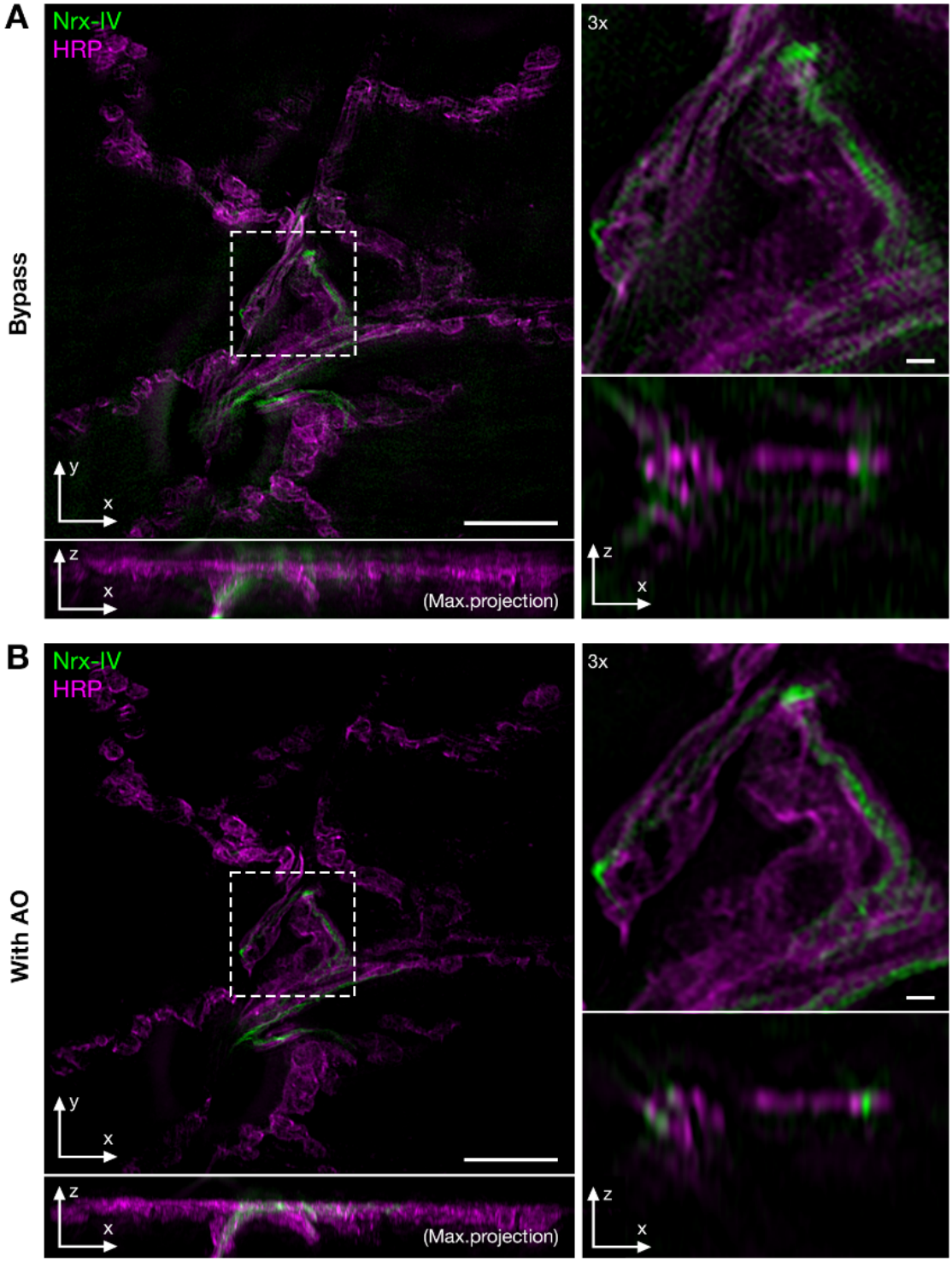

Figure 3. Aberration correction using adaptive optics (AO) removes artefacts and improves contrast and resolution of 3D-SIM images of neuromuscular junction in a fixed L3 *Drosophila* larva. The images show Nrx-IV::GFP expression in green and anti-
625 body staining of neuronal membranes with anti-HRP in magenta. Panels A and B show the following images from the 3D images acquired without (A) and with AO (B) respectively: top-

left, maximum projection of the acquired volumes; bottom-left, XZ view along Y drawn at the image center; top-right , 3× zoom of the boxed area in XY view; bottom right, XZ view of the zoomed area along Y at the image center. Total volume is $63.36 \times 63.36 \times 8.75$ μm. Scale bar is 20 μm.

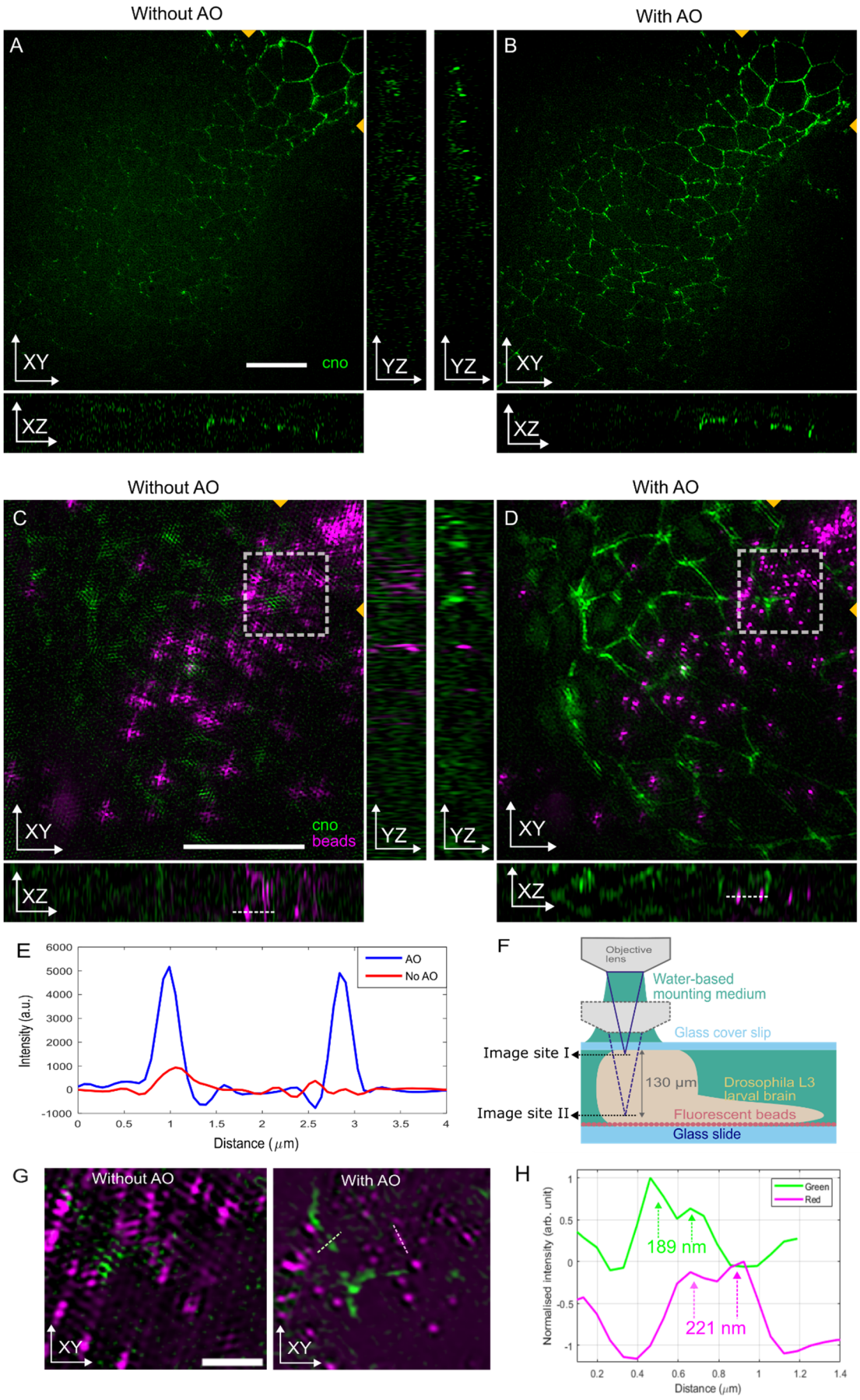
Without AO
With AO
A
B
XY
YZ
XZ
cno
C
D
cno
beads
E
AO
No AO
Intensity (a.u.)
Distance (μm)
F
Objective lens
Water-based mounting medium
Glass cover slip
Image site I
Image site II
130 μm
Drosophila L3 larval brain
Fluorescent beads
Glass slide
G
H
Green
Red
189 nm
221 nm
Normalised intensity (arb. unit)
Distance (μm)

Figure 4. 3D-SIM is made possible in deep tissue samples by correcting aberrations with adaptive optics (AO). A-B, 3D-SIM images of fixed Drosophila L3 larval brain, mounted and imaged from top downwards, at a depth of 3 μm measured from lower surface of coverslip without AO (A) and with AO (B) with XZ and YZ orthogonal views along the lines indicated by the golden arrowheads shown below and besides. The green channel showed cno::YFP expression at the adherent junctions between neuroepithelial stem cells in the outer proliferation centers in the optic lobes. C-D, 3D-SIM images of the same fixed Drosophila L3 larval brain, through the entire volume of a single brain lobe, at 130 μm from top surface without AO (C) and with AO (D) with XZ and YZ orthogonal views along the lines indicated by the golden arrowheads shown below and besides; E plots the image intensities in the red channel along the dotted line in the XZ views in C and D, which clearly shows peak intensity improvement with AO correction; F, drawing illustrates the way that the specimen was mounted and imaged. The larval brain was mounted in PBS between a glass cover slip (top) and a glass slide (bottom); the slide was coated with medium density red fluorescent beads (100 nm diameter). G, Zoomed-in display of boxed areas in C and D, H plots the image intensity in the red channel along the dotted line in G, which shows around 200 nm resolution at an extreme imaging depth with AO correction; the same information cannot be restored from the images acquired without AO. Imaged volumes were 59.14 x 59.14 x 9.75 μm^3 μm^3 (A and B), 29.57 x 29.57 x 4.88 μm^3 (C and D), and 6.7 x 6.7 μm^2 (G). Scale bars are 10 μm (A-D) and 2 μm (G).

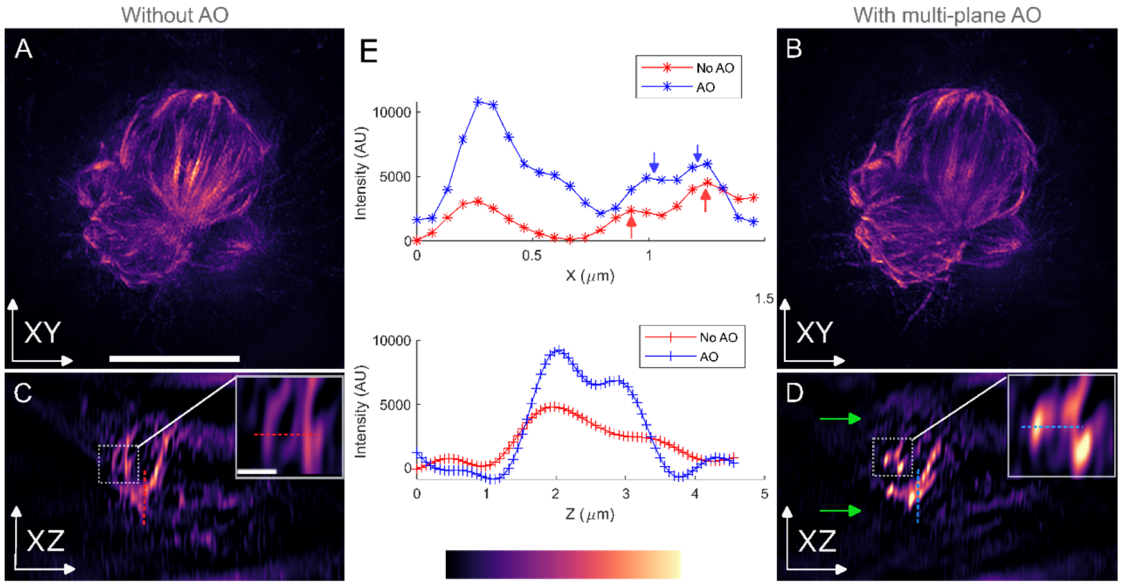

Figure 5. Multi-plane aberration correction improves 3D-SIM resolution and contrast over a large volume. Spindle fibers in COS-7 cells were stained with Alexa Fluor 488, visualizing the microtubule cytoskeleton. The volumes were acquired with remote focusing. Aberration measurements were performed at two imaging planes, one on the top the other on the bottom of the cell volume (indicated by green arrows in D); dynamic correction was applied for all intermediate planes where images were acquired with 125 nm Z steps. Panels A and B show maximum projection without and with AO. Panels C and D show XZ cross-section view without and with AO, along the lines indicated by the golden arrowheads appear in A and B; central areas of C and D in the dotted box are displayed with 3× zoom on the top-right corner; green arrows in D indicate the two positions for aberration measurements. Panel E displays plots of image pixel value along X and Z direction drawn in Panel C (in red) and D (in blue), from which the peak signal and the resolution are both enhanced by adopted multi-plane AO. Scale bar is 10 μm in A-D except that in the 3× zoom-in areas in C and D where scale bar is 1 μm.

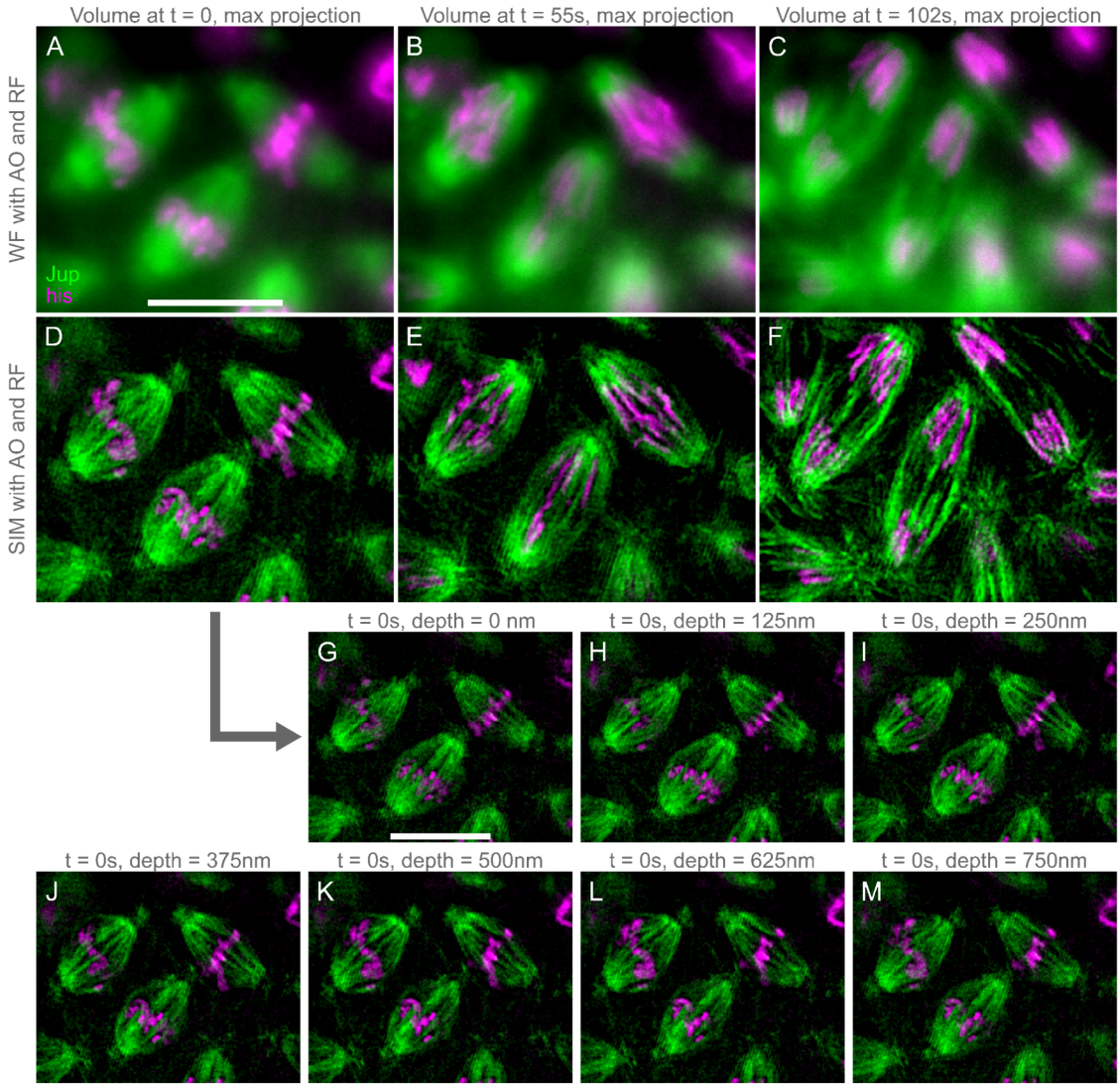

Figure 6. Remote focusing enables live 3D-SIM time-lapse imaging in *Drosophila* syncytial blastoderm embryos. The mitotic embryonic divisions are visualized using transgenic Jupiter::GFP that label microtubules in green and transgenic Histone::RFP visualizing chromosomes in magenta. Panels A-C and D-F show maximum projections of three different time points of wide-field and 3D-SIM reconstructions of the same 3D+t data, respectively. Panels G-M show the separate sections of D. Scale bar: 10 µm.

References

Antonello, J., J. Wang, C. He, M. Phillips, and M. Booth. 2020. Interferometric calibration of a deformable mirror. *Zenodo. 2020b doi*. 10.

Ball, G., J. Demmerle, R. Kaufmann, I. Davis, I.M. Dobbie, and L. Schermelleh. 2015. SIMcheck: a toolbox for successful super-resolution structured illumination microscopy. *Scientific reports*. 5:15915.

Bitenc, U., N.A. Bharmal, T.J. Morris, and R.M. Myers. 2014. Assessing the stability of an ALPAO deformable mirror for feed-forward operation. *Optics express*. 22:12438-12451.

Brent, J.R., K.M. Werner, and B.D. McCabe. 2009. Drosophila larval NMJ dissection. *JoVE (Journal of Visualized Experiments)*:e1107.

Corbett, A.D., M. Shaw, A. Yacoot, A. Jefferson, L. Schermelleh, T. Wilson, M. Booth, and P.S. Salter. 2018. Microscope calibration using laser written fluorescence. *Optics express*. 26:21887-21899.

Demmerle, J., C. Innocent, A.J. North, G. Ball, M. Müller, E. Miron, A. Matsuda, I.M. Dobbie, Y. Markaki, and L. Schermelleh. 2017. Strategic and practical guidelines for successful structured illumination microscopy. *Nature Protocols*. 12:988-1010.

Gao, L., L. Shao, C.D. Higgins, J.S. Poulton, M. Peifer, M.W. Davidson, X. Wu, B. Goldstein, and E. Betzig. 2012. Noninvasive imaging beyond the diffraction limit of 3D dynamics in thickly fluorescent specimens. *Cell*. 151:1370-1385.

Gustafsson, M.G., L. Shao, P.M. Carlton, C.J. Wang, I.N. Golubovskaya, W.Z. Cande, D.A. Agard, and J.W. Sedat. 2008. Three-dimensional resolution doubling in wide-field fluorescence microscopy by structured illumination. *Biophys J*. 94:4957-4970.

Hailstone, M., D. Waithe, T.J. Samuels, L. Yang, I. Costello, Y. Arava, E. Robertson, R.M. Parton, and I. Davis. 2020. CytoCensus, mapping cell identity and division in tissues and organs using machine learning. *Elife*. 9:e51085.

Hall, N. 2020. Chapter 3.2. 2 'Accessible adaptive optics and super-resolution microscopy to enable improved imaging'. Ph. D. thesis, University of Oxford.

Hall, N., J. Titlow, M.J. Booth, and I.M. Dobbie. 2020. Microscope-AOtools: a generalised adaptive optics implementation. *Optics Express*. 28:28987-29003.

Huang, B., M. Bates, and X. Zhuang. 2009. Super-resolution fluorescence microscopy. *Annual review of biochemistry*. 78:993-1016.

KAM, Z., P. KNER, D. AGARD, and J.W. SEDAT. 2007. Modelling the application of adaptive optics to wide-field microscope live imaging. *Journal of Microscopy*. 226:33-42.

Kner, P., Z. Kam, D. Agard, and J. Sedat. 2011. Adaptive optics in wide-field microscopy. SPIE.

Kounatidis, I., M.L. Stanifer, M.A. Phillips, P. Paul-Gilloteaux, X. Heiligenstein, H. Wang, C.A. Okolo, T.M. Fish, M.C. Spink, and D.I. Stuart. 2020. 3D correlative cryo-structured illumination fluorescence and soft X-ray microscopy elucidates reovirus intracellular release pathway. *Cell*. 182:515-530. e517.

Li, Q., M. Reinig, D. Kamiyama, B. Huang, X. Tao, A. Bardales, and J. Kubby. 2017. Woofer–tweeter adaptive optical structured illumination microscopy. *Photon. Res.* 5:329-334.

Lin, R., E.T. Kipreos, J. Zhu, C.H. Khang, and P. Kner. 2021. Subcellular three-dimensional imaging deep through multicellular thick samples by structured illumination microscopy and adaptive optics. *Nature Communications*. 12:3148.

Matsuda, A., T. Koujin, L. Schermelleh, T. Haraguchi, and Y. Hiraoka. 2020. High-accuracy correction of 3d chromatic shifts in the age of super-resolution biological imaging using chromagnon. *JoVE (Journal of Visualized Experiments)*:e60800.
Mertz, J., H. Paudel, and T.G. Bifano. 2015. Field of view advantage of conjugate adaptive optics in microscopy applications. *Applied optics*. 54:3498-3506.
Ogushi, S., A. Rattani, J. Godwin, J. Metson, L. Schermelleh, and K. Nasmyth. 2021. Loss of sister kinetochore co-orientation and peri-centromeric cohesin protection after meiosis I depends on cleavage of centromeric REC8. *Developmental cell*. 56:3100-3114. e3104.
Parton, R.M., A.M. Vallés, I.M. Dobbie, and I. Davis. 2010. Live cell imaging in Drosophila melanogaster. *Cold Spring Harbor Protocols*. 2010:pdb. top75.
Phillips, M.A., M. Harkiolaki, D.M.S. Pinto, R.M. Parton, A. Palanca, M. Garcia-Moreno, I. Kounatidis, J.W. Sedat, D.I. Stuart, and A. Castello. 2020. CryoSIM: super-resolution 3D structured illumination cryogenic fluorescence microscopy for correlated ultrastructural imaging. *Optica*. 7:802-812.
Phillips, M.A., D.M. Susano Pinto, N. Hall, J. Mateos-Langerak, R.M. Parton, J. Titlow, D.V. Stoychev, T. Parks, T. Susano Pinto, and J.W. Sedat. 2022. Microscope-Cockpit: Python-based bespoke microscopy for bio-medical science. *Wellcome Open Research*. 6:76.
Poland, S.P., A.J. Wright, and J.M. Girkin. 2008. Active focus locking in an optically sectioning microscope utilizing a deformable membrane mirror. *Opt. Lett.* 33:419-421.
Richter, V., M. Piper, M. Wagner, and H. Schneckenburger. 2019. Increasing resolution in live cell microscopy by structured illumination (SIM). *Applied Sciences*. 9:1188.
Sahl, S.J., S.W. Hell, and S. Jakobs. 2017. Fluorescence nanoscopy in cell biology. *Nature reviews Molecular cell biology*. 18:685-701.
Schermelleh, L., P.M. Carlton, S. Haase, L. Shao, L. Winoto, P. Kner, B. Burke, M.C. Cardoso, D.A. Agard, and M.G. Gustafsson. 2008. Subdiffraction multicolor imaging of the nuclear periphery with 3D structured illumination microscopy. *science*. 320:1332-1336.
Schermelleh, L., A. Ferrand, T. Huser, C. Eggeling, M. Sauer, O. Biehlmaier, and G.P. Drummen. 2019. Super-resolution microscopy demystified. *Nature cell biology*. 21:72-84.
Schermelleh, L., R. Heintzmann, and H. Leonhardt. 2010. A guide to super-resolution fluorescence microscopy. *Journal of Cell Biology*. 190:165-175.
Schindelin, J., I. Arganda-Carreras, E. Frise, V. Kaynig, M. Longair, T. Pietzsch, S. Preibisch, C. Rueden, S. Saalfeld, and B. Schmid. 2012. Fiji: an open-source platform for biological-image analysis. *Nature methods*. 9:676-682.
Susano Pinto, D.M., M.A. Phillips, N. Hall, J. Mateos-Langerak, D. Stoychev, T. Susano Pinto, M.J. Booth, I. Davis, and I.M. Dobbie. 2021. Python-Microscope–a new open-source Python library for the control of microscopes. *Journal of Cell Science*. 134:jcs258955.
Temma, K., R. Oketani, T. Kubo, K. Bando, S. Maeda, K. Sugiura, T. Matsuda, R. Heintzmann, T. Kaminishi, and K. Fukuda. 2023. Selective plane activation structured illumination microscopy. *bioRxiv*:2023.2006. 2019.545558.
Thomas, B., A. Wolstenholme, S.N. Chaudhari, E.T. Kipreos, and P. Kner. 2015. Enhanced resolution through thick tissue with structured illumination and adaptive optics. *Journal of biomedical optics*. 20:026006-026006.
Turcotte, R., Y. Liang, M. Tanimoto, Q. Zhang, Z. Li, M. Koyama, E. Betzig, and N. Ji. 2019. Dynamic super-resolution structured illumination imaging in the living brain. *Proceedings of the National Academy of Sciences*. 116:9586-9591.

Wang, J., E.S. Allgeyer, G. Sirinakis, Y. Zhang, K. Hu, M.D. Lessard, Y. Li, R. Diekmann, M.A. Phillips, and I.M. Dobbie. 2021. Implementation of a 4Pi-SMS super-resolution microscope. *Nature protocols*. 16:677-727.

Wang, J., and Y. Zhang. 2021. Adaptive optics in super-resolution microscopy. *Biophysics Reports*. 7:267.

Wang, Y., Z. Yu, C.K. Cahoon, T. Parmely, N. Thomas, J.R. Unruh, B.D. Slaughter, and R.S. Hawley. 2018. Combined expansion microscopy with structured illumination microscopy for analyzing protein complexes. *Nature Protocols*. 13:1869-1895.

Žurauskas, M., O. Barnstedt, M. Frade-Rodriguez, S. Waddell, and M.J. Booth. 2017. Rapid adaptive remote focusing microscope for sensing of volumetric neural activity. *Biomedical optics express*. 8:4369-4379.

Žurauskas, M., I.M. Dobbie, R.M. Parton, M.A. Phillips, A. Göhler, I. Davis, and M.J. Booth. 2019. IsoSense: frequency enhanced sensorless adaptive optics through structured illumination. *Optica*. 6:370-379.